Friction **11**(2): 246–258 (2023)
https://doi.org/10.1007/s40544-022-0598-5
ISSN 2223-7690
CN 10-1237/TH

RESEARCH ARTICLE

Tribological properties of hierarchical micro-dimples produced on a cylindrical surface by dual-frequency texturing

Saood ALI, Rendi KURNIAWAN*, Park Gun CHUL, Tae Jo KO*
School of Mechanical Engineering, Yeungnam University, Gyeongsan-si 712749, Republic of Korea
Received: 03 May 2021 / Revised: 15 July 2021 / Accepted: 08 January 2022

Abstract: An experimental investigation was performed for investigating the tribological performance of micro-dimple surface texture patterns on a cylindrical surface in a realistic operating environment of starved lubrication. Micro-dimples were generated by a dual-frequency surface texturing method, in which a high-frequency (16.3 kHz) three-dimensional (3D) vibration and a low-frequency (230 Hz) one-dimensional (1D) vibration were applied at the tool tip simultaneously, resulting in the generation of the hierarchical micro-dimples in a single step. Rotating cylinder-on-pin tribological tests were conducted to compare the tribological performance of the non-textured reference specimen and micro-dimple samples. The effect of surface textures generated with various shape parameters (long drop and short drop), dimension parameters (length and surface texture density), and operation parameters (load and sliding velocity) on the tribological performance was evaluated. Stribeck curves indicate that the hierarchical micro-dimples exhibit a lower coefficient of friction than the reference specimen in the high contact-pressure regions. It is also observed that variation in the length of a micro-dimple, the shape effect, is the major factor affecting the friction response of the textured surfaces. The generation of additional hydrodynamic pressure and lift effect by hierarchical structures is the main reason for the improved performance of hierarchical micro-dimple surfaces.

Keywords: dual-frequency surface texturing; hierarchical surfaces; tribology; starved lubrication; three-dimensional elliptical vibration transducer

1 Introduction

Nature often uses multi-scale hierarchical surfaces to enhance the physical properties [1]. The most studied phenomenon regarding this is the reduction in drag effect by shark and dolphin skin due to the presence of micro-features at two different scales [2]. Also, in the case of lotus leaves, surface roughness at different scales combine to achieve self-cleaning properties and a super-hydrophobic effect [3]. Inspired by these natural instances of animals and plants, researchers are developing textured surfaces at multiple scales to take advantage of their benefits for improving the tribological performance of components by reducing friction and wear [4].

Initially, the systematic work highlighting the effect of surface textures on the tribological performances of different machine components (seals and piston rings) in different lubrication conditions are carried out by Etsion and co-workers [5]. Subsequently, this topic has gained tremendous interest and focus from tribologists. In the past two decades, several articles have been published on the state of the art regarding the influence of surface texturing on friction and wear in laboratory experiments and machine components [6]. However, interestingly, a majority of these studies highlight the effect of only single-scale textures.

The idea of transferring the multi-scale hierarchical surface texture phenomenon in nature to a real-world engineering application has been gaining around

* Corresponding authors: Tae Jo KO, E-mail: tjko@yu.ac.kr; Rendi KURNIAWAN, E-mail: rendi@ynu.ac.kr

since last decade. The generation of hierarchical surface textures efficiently and accurately is important since textures of all scales should be combined suitably and should be left intact during a texturing process. As for textured surfaces, in general and particularly for hierarchical textured surfaces, the tribological properties are significantly influenced by the surface textures features [7].

Of the vast number of available methods, laser surface texturing was initially used for hierarchical surface texture generation [8]. But the requirements of costly equipment, a controlled environment, and collateral damage to the surrounding material were some of the reasons that forced researchers to develop a new method for hierarchical texture generation [9]. Elliptical vibration texturing (EVT) is a modified form of elliptical vibration cutting (EVC), and has been used successfully in recent times for creating a hierarchical structure in a single step operation, which reduces the operation cost and time and increases the texturing efficiency by many times [10].

Zhou et al. [11] first generated hierarchical structures using a double frequency elliptical vibration cutting method employing a two-dimensional (2D) non-resonant vibration transducer on a conventional fast tool servo. However, it inherits the disadvantages of a conventional fast tool servo method that were experienced by a number of researchers. Yuan et al. [12] used a double frequency vibration cutting system and generated hierarchical structures on a flat hardened steel workpiece by employing a 2D resonant ultrasonic vibrator and a 1D non-resonant compliant vibrator simultaneously. Guo et al. [13] used a 2D elliptical vibration texturing method to generate hierarchical structures on cylindrical surfaces. Kurniawan et al. [14] used a two-frequency vibration device for surface texturing and achieved improved surface roughness compared to the conventional surface texturing method.

As summarized above, a number of experimental methods have been used successfully to generate hierarchical structures on flat or cylindrical surfaces in a single-step operation. But as observed with the available methods, it is not possible to manufacture the hierarchical micro-dimples with a depth of more than 10 μm, especially on cylindrical specimens. Moreover, despite the importance of the effect of the hierarchical structures on the hydrodynamic pressure and friction, the tribological performance of hierarchical texture surfaces with different geometrical features under realistic lubrication conditions, such as starved boundary lubrication, remains unexplored.

Therefore, the objective of the present study is to explore the idea of using the hierarchical micro-dimples to improve the tribological performance of cylindrical surfaces under starved lubrication conditions. The novelty of this research is in understanding the effect of the hierarchical micro-dimples in dictating the friction characteristics of the micro-dimple textured surfaces in a starved lubrication environment to provide effective boundary lubrication during manufacturing or in the operation of mechanical components. Even though the effects of various surface textures on lubrication mechanisms have been studied in detail in the past, the effect of hierarchical micro-structures on the friction performance of surface texture parameters, such as texture density and micro-dimple shape, is still an underexplored area of research in the case of the hierarchical micro-dimples. In this study, a hierarchical micro-dimple textured surface was generated using a novel dual-frequency texturing method, employing a 3D resonant elliptical vibration transducer, under different rotational speeds. And then, the friction performance of the hierarchical micro-dimples was analyzed with respect to a non-textured reference specimen under different sliding speed, applied load, and geometrical shape conditions. The presence of shape effect in the form of micro-dimple length was identified as the key parameter responsible for the frictional performance of the hierarchical micro-dimples under starved lubrication conditions.

2 Dual-frequency surface texturing: Principle of operation

The idea of combining 1D conventional texturing (CT) and elliptical vibration cutting (EVC) results in the generation of a dual-frequency surface texturing method. In the dual-frequency surface texturing method, 1D CT was achieved using a low-frequency displacement amplifier, and a 3D elliptical vibration transducer was developed for EVC (Fig. 1) [15]. The

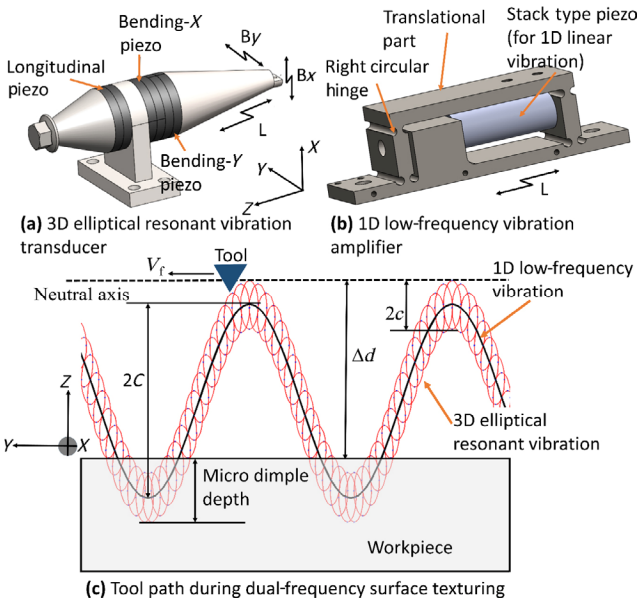

Fig. 1 (a) 3D resonant vibration transducer, (b) 1D low-frequency displacement amplifier, and (c) tool tip path locus during dual-frequency surface texturing operation.

3D elliptical vibration transducer is a symmetrical sandwich type and has a resonant frequency of 16.3 kHz for vibrations in a 3D space, as shown in Fig. 1(a).

The relative motion of the tool tip in a 3D Cartesian coordinate system using a dual-frequency surface texturing method can be expressed using Eqs. (1), (2), and (3):

$$x(t) = a \cdot \cos(2\pi f_h + \varphi_{Bx}) \tag{1}$$

$$y(t) = b \cdot \cos(2\pi f_h + \varphi_{By}) + V_f \cdot t \tag{2}$$

$$z(t) = c \cdot \cos(2\pi f_h + \varphi_L) + C \cdot \cos(2\pi f_l \cdot t) \tag{3}$$

$$2\pi f_h \cdot b > V_f \tag{4}$$

where $x(t)$, $y(t)$, and $z(t)$ are the positions of the tool tip in a 3D Cartesian coordinate system, f_h is the high 3D resonance frequency (≈ 16.3 kHz), f_l is the one-dimensional low-frequency of a sinusoidal wave (≈ 230 Hz), φ_{Bx}, φ_{By}, and φ_L are phase shifts, and V_f is the nominal relative cutting velocity. The 3D elliptical locus of the tool tip has amplitudes of a, b, and c in the x-, y-, and z-directions, respectively, while C is the amplitude of the low-frequency 1D sinusoidal wave. Equation (4) represents the condition of intermittent cutting during micro-dimple surface texturing. The spindle speed is selected in such a way that this condition always remains true.

The trajectory of the transducer tip superimposed with low-frequency 1D vibration and high-frequency 3D resonant vibration is shown in Fig. 1(c). It was observed that the primary profile of the micro-dimple depends on the low-frequency vibration, while the high-frequency 3D resonant vibration is responsible for the nano-textures in the primary profile. The nano-texture configuration in the primary profile depends on the 3D elliptical locus of the tool tip at the 3D resonant vibration frequency.

3 Experimental details

3.1 Workpiece material selection

Al6061 aluminum alloy is widely used in applications that specifically demand high strength-to-weight ratio, low density, high specific strength, and good formability [16, 17]. Due to these properties, Al6061–T6 has applications in the manufacturing of aviation structures, such as wings and fuselages, and in the automobile industry for making engine parts, such as chassis, pistons, and crankshafts [18, 19]. However, the main drawback of Al6061–T6 is that it exhibits poor tribological performance under adverse operating conditions, such as starved or dry lubrication conditions, which limits its further use [20, 21].

In the present study, an Al6061–T6 alloy workpiece in the form of a cylindrical specimen was selected as the working material. The workpiece material composition is shown in Table 1. Initially, the workpiece was machined to a diameter of 28 mm with an average surface roughness of $Ra \approx 0.5$ μm. Surface textures in the form of a micro-dimple pattern were then created on

Table 1 Chemical composition of Al6061–T6 alloy.

Serial No.	Component	Chemical composition (wt%)
1	Chromium (Cr)	0.04–0.35
2	Copper (Cu)	0.15–0.40
3	Magnesium (Mg)	0.80–1.20
4	Silicon (Si)	0.40–0.80
5	Manganese (Mn)	0.15 max.
6	Titanium (Ti)	0.15 max.
7	Zinc (Zn)	0.25 max.
8	Iron (Fe)	0.70 max.
9	Aluminum (Al)	Balance

the surface using the dual-frequency surface texturing method.

3.2 Machining conditions

The experimental platform was fixed on a computer numerical control lathe machine manufactured by Daegu Heavy Inc. Co., Ltd., Republic of Korea, which has a resolution of 1 μm, as shown in Fig. 2. The whole experimental setup consisted of two devices: a single-excitation 3D elliptical vibration transducer and a displacement amplifier. The vibration parameters of the experimental setup are presented in Table 2.

The 3D resonant vibration frequency was found to be 16.3 kHz with phase differences of 0°, 45°, and 90° between the longitudinal, bending-x, and bending-y directions, respectively. The 1D low vibration frequency was fixed at 230 Hz as the transducer had the highest displacement amplitude at a frequency of 230 Hz. The distance between the tool tip and the workpiece before starting the surface texturing was designated as Δd in Fig. 1(c), and was set as 5 μm to obtain clear and distinguishable micro-dimples. The tool used during surface texturing was an inexpensive polycrystalline diamond (PCD) insert tip with a triangular shape, as shown in Fig. 2. The machining parameters for the non-textured specimen and the texturing operation are given in Table 3.

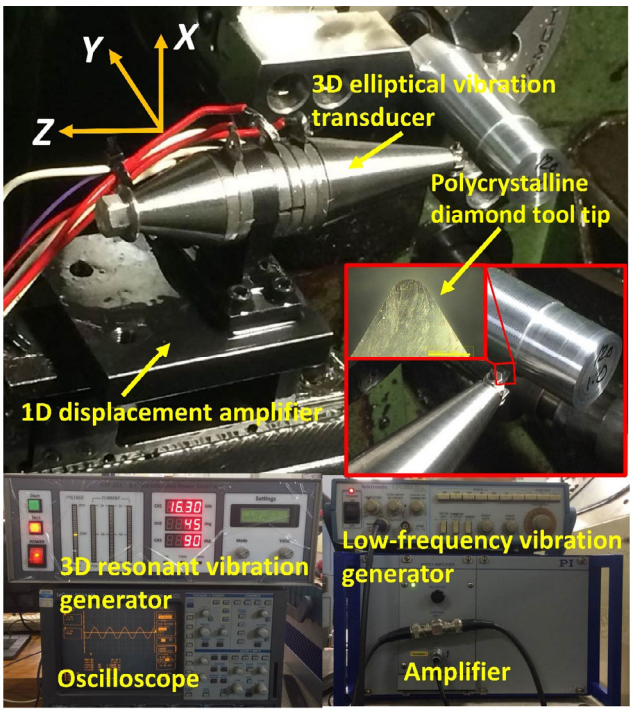

Fig. 2 Experimental setup for dual-frequency surface texturing.

Table 2 Vibration parameters of the experimental setup.

Low vibration frequency (f_l)	230 Hz	
Low vibration frequency amplitude	22.5 μm	
3D resonant vibration frequency (f_h)	16.3 kHz	
Phase shift at 3D resonant vibration (φ_L, φ_{Bx}, and φ_{By})	0°, 45°, and 90°	
3D elliptical locus amplitude	Longitudinal	1.5 μm
	Bending-x	2.7 μm
	Bending-y	5.2 μm

Table 3 Machining parameters.

Workpiece material	Al6061–T6		
Diameter	28 mm		
Tool type	Polycrystalline diamond (PCD)		
Surface roughness of non-textured specimen	$Ra \leq 0.51 \pm 0.012$ μm		
Surface texturing operation	Feed rate (mm/r)		0.6
			0.8
			1.0
	Spindle speed during surface texturing (r/min)	Case 1	60
		Case 2	80
		Case 3	100
		Case 4	120
		Case 5	140

3.3 Surface texture density

First, the non-textured specimen was made at a spindle speed of 450 r/min, so the average surface roughness of the non-textured specimen should be approximately $Ra \approx 0.5$ μm. The textured surfaces were generated with three feed rate values of 0.6, 0.8, and 1.0 mm/r. The feed rate values were selected in such a way that the surface texture density remained between the limits of 15% and 30%. The surface texture density was calculated using Eq. (5). The variation in the surface texture density with respect to the feed rate value is shown in Fig. 3.

$$S_d(\%) = \frac{\text{Total No. of dimples in one revolution} \times \text{Area of one dimple}}{\text{Total area covered in one revolution}} \times 100\% \quad (5)$$

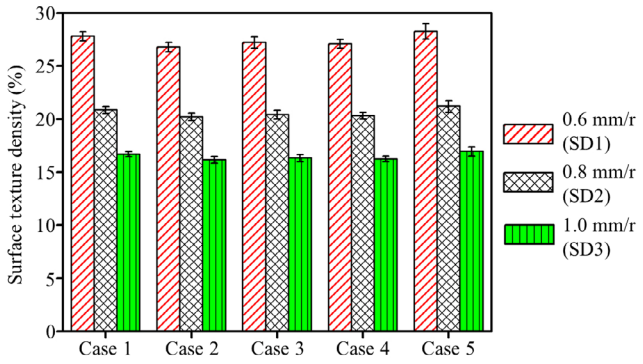

Fig. 3 Effects of feed rate and spindle speed during surface texturing on surface texture density.

The surface texture density at a given feed rate value does not change with the change in spindle speed during surface texturing and remains constant (Fig. 3). The reason for this is that although the number of micro-dimples in one revolution changes with spindle speed, the corresponding change in the single micro-dimple area overcomes this change in the number of micro-dimples. Therefore, overall, the surface texture density is mainly affected by the feed rate value, while the spindle speed does not affect the texture density for the cylindrical workpiece surface texturing.

3.4 Micro-dimple geometric parameters

Surface texture patterns in the form of five different micro-dimples were made successfully on a cylindrical surface by varying the spindle speed during surface texturing from 60 to 140 r/min in steps of 20 r/min. The spindle speed during surface texturing was chosen in such a way that the condition of intermittent cutting, given in Eq. (4) would always be met during micro-dimple generation using the dual-frequency method. At a given feed rate value, the axial distance between the two successive rows of micro-dimples remained constant, irrespective of the spindle speed, and it was equal to the feed rate value.

The diameter of the micro-dimples depends on the geometric properties of the cutting tool, and there is not much effect on the micro-dimple diameter with a change in spindle speed. However, the variation in spindle speed changes the micro-dimple shape from a short drop to a long drop due to a substantial increase in the micro-dimple length. In addition, the circumferential distance increases between two successive micro-dimples, which is named as the micro-dimple pattern's cross pitch. A 3D surface profilometer (Nano-map E-series) was used to capture images of all the micro-dimple patterns. The texture patterns generated at different feed rate values are shown in Fig. 4.

A micro-dimple profile along the feed and cutting direction is shown in Fig. 5 for all the cases. The diameter of the micro-dimple is represented by the profile along the feed direction, while the micro-dimple profile along the cutting direction shows the length of the micro-dimple. Geometric parameters of the micro-dimple patterns at different feed rate values are shown in Fig. 6. A scanning electron microscopy (SEM) analysis was performed to capture the hierarchical vibration patterns inside a micro-dimple, as shown in Fig. 7.

Hierarchical micro-dimples contain secondary micro-nano structures inside the primary profile generated by 3D resonant high frequency vibration. Low frequency only micro-dimples do not have any micro-nano structures inside their primary profile.

The micro-morphologies of the different surfaces (non-textured surface, hierarchical micro-dimple textured surface, and low-frequency only micro-dimple textured surface) were analyzed using SEM, as illustrated in Fig. 8. The chemical composition of the different surfaces was also analyzed using energy dispersive X-ray spectroscopy (EDS). The elemental distribution was effectively represented by the EDS results, as shown in Figs. 8(a)–8(c). It was observed that the micro-dimple surface texturing using the dual-frequency method did not affect the surface characteristics, which was a common outcome in the

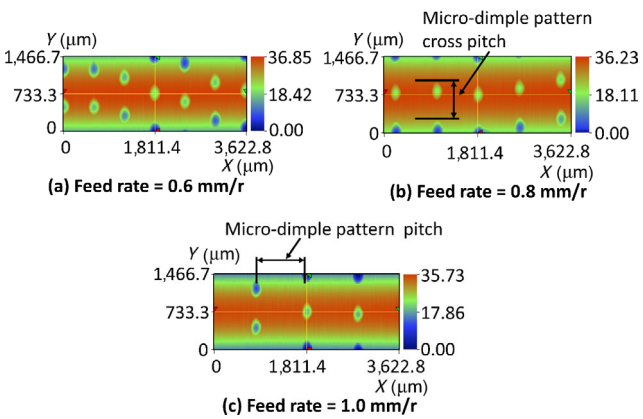

Fig. 4 Surface texture patterns at different feed rate values.

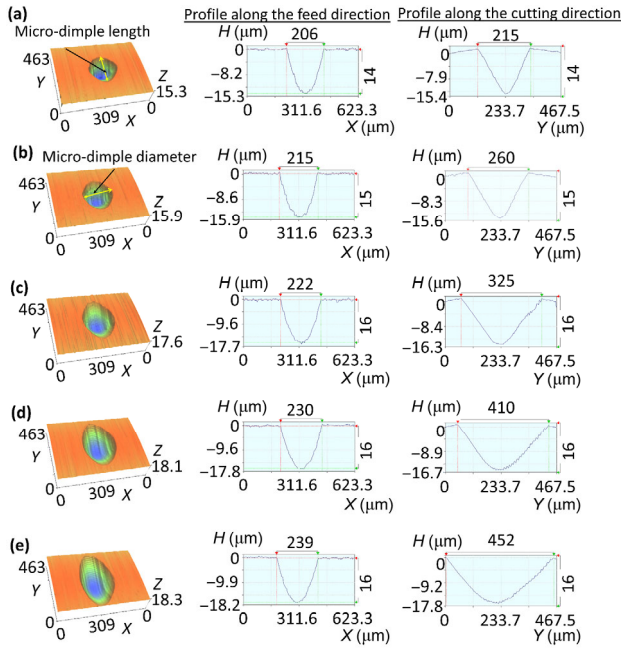

Fig. 5 Effect of spindle speed on micro-dimple shape and micro-dimple profiles along the feed and cutting directions: (a) Case 1, (b) Case 2, (c) Case 3, (d) Case 4, and (e) Case 5.

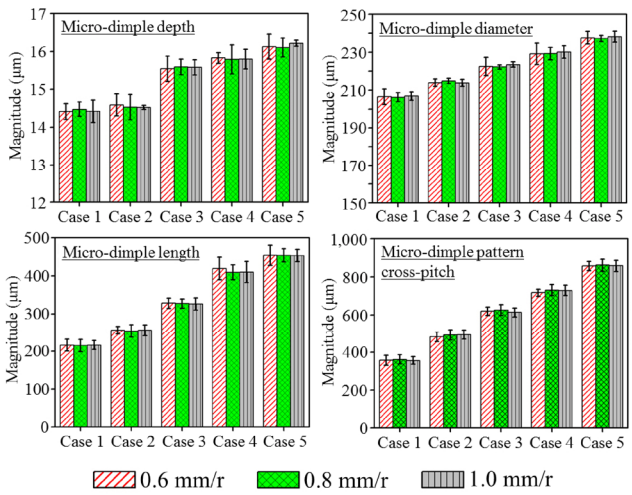

Fig. 6 Micro-dimple geometric parameters.

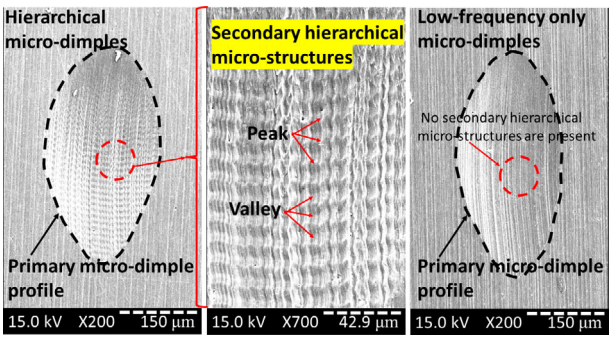

Fig. 7 Difference between the dual-frequency surface textured micro-dimple and the low-frequency only micro-dimple.

case of coating and laser surface-texturing methods [22, 23]. The major element of the Al6061–T6 alloy was observed in the EDS analysis, and no foreign inclusion of any other element was observed [24]. Therefore, the use of machining-based methods, such as the dual-frequency method for surface texturing did not need further chemical examination of the surface as there were no changes in the surface chemical properties. The only changes that were observed were physical parameters of the textured surfaces resulting from variation in texturing speed and feed rate values.

3.5 Tribological experiment

The tribological properties of the cylindrical specimens were measured using a commercial tribometer (Hanmi Industries Corp., Republic of Korea) in a block-on-ring configuration. A schematic diagram of the block-on-ring tribometer is shown in Fig. 9(a). During testing, the stationary block was pressed with a constant load against a rotating cylindrical specimen and had its axis perpendicular to the axis of rotation of the specimen. The stationery block is made of AISI 52100 steel, which has an average surface roughness of Ra = 0.2 μm. The geometric configuration of the stationary block is shown in Fig. 9(b). The Rockwell hardness of the stationary block and the rotating specimen are HRC = 60 and HRB = 50, respectively, so a Hertzian contact pressure in the range of 30 MPa–1.0 GPa can be achieved between the contacting surfaces.

The direction of the sliding motion relative to the textured pattern is shown in Fig. 10. During the tribological test, the normal load and friction force between the sliding surfaces of the block and the cylindrical specimen were monitored, and the friction coefficient was computed in real time. The friction test was of a constant sliding distance type with varied sliding times according to the sliding speed. The influences of the variation in the sliding speed and normal load on the friction behavior of the cylindrical specimen were analyzed.

The tribology tests were conducted on all the specimens at 10 levels of sliding speed and three levels of applied load: L_1 = 10 N, L_2 = 30 N, and L_3 = 50 N. The tribological tests were performed in a starved lubrication environment. Starved lubrication was

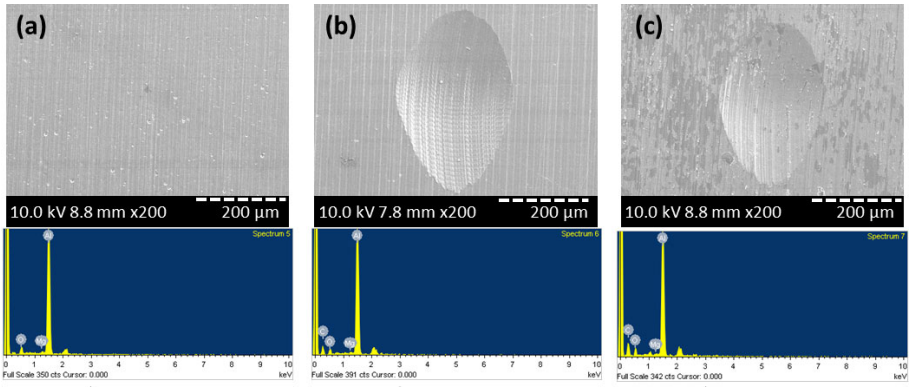

Element	Weight (%)	Atomic (%)
C K	16.71	2.53
O K	8.27	15.29
Al K	75.02	82.18
Total	100.00	

Element	Weight (%)	Atomic (%)
C K	23.13	28.82
O K	7.26	9.15
Al K	69.61	52.02
Total	100.00	

Element	Weight (%)	Atomic (%)
C K	31.18	48.11
O K	9.78	11.33
Al K	59.04	40.55
Total	100.00	

Fig. 8 Micro-morphology of different surfaces: (a) non-textured surface, (b) hierarchical micro-dimple textured surface, and (c) low-frequency only micro-dimple textured surface.

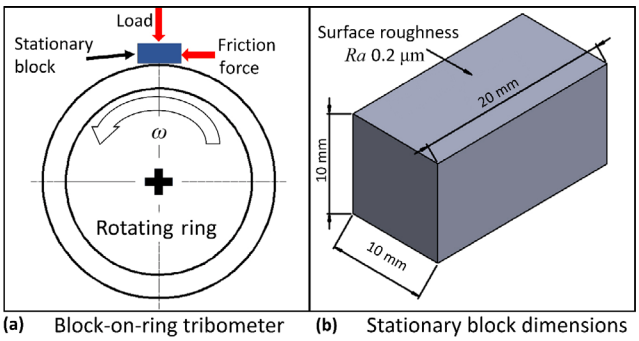

Fig. 9 (a) Diagram of block-on-ring tribometer configuration and (b) stationary block geometrical configuration.

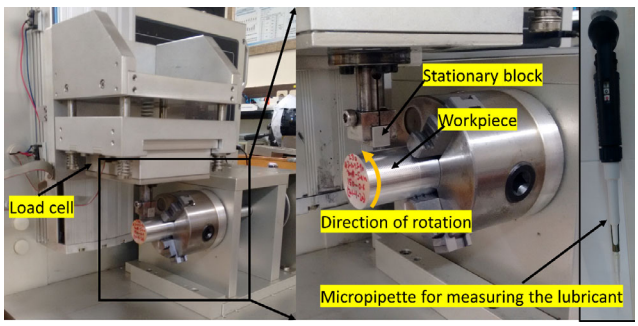

Fig. 10 Block-on-ring tribometer setup for friction test.

simulated by applying a minuscule amount of lubricant directly to the contact region. The amount of lubricant was quantified in terms of the volume of the lubricant at the contact region, which was only 20 µL for the lubricant used in the present experiment. With such a minuscule amount of lubricant at the contact region, the operating regime was closer to boundary lubrication instead of mixed lubrication, so it was termed as starved lubrication. A commercially available liquid lubricant that has an ISO viscosity grade of VG68, a density of 0.878 g/cm^3, and a dynamic viscosity of 0.15804 Pa·s at room temperature (25 °C) was used as a lubricant during the experiment.

4 Results and discussion

In this section, the behaviors of micro-dimple textured surfaces with different shapes, different texture densities, and different contact pressures under starved lubrication conditions are presented. The Hertzian contact pressures created between the interacting surfaces during the tribology tests were 36 MPa at 10 N, 62 MPa at 30 N, and 81 MPa at 50 N of applied loads. The tribology tests were repeated three times for each condition; consequently, the average friction coefficient was calculated. Stribeck curves comparing the friction coefficients of the non-textured reference specimen and the textured specimens are presented.

4.1 Influence of micro-dimple shape

Micro-dimples with five different shapes that have different micro-dimple lengths were generated by

controlling the spindle speed during the surface texturing, as shown in Fig. 6. The micro-dimple shape changes from a short-drop type to a long spherical drop type as the spindle speed increases. The effect of the micro-dimple shape on the friction coefficient at a constant contact pressure condition with respect to the non-textured reference specimen is shown in Fig. 11.

Figure 11(a) shows the friction coefficient variation at a contact pressure of 36 MPa. It is observed that in the low contact-pressure region, the friction coefficient variation moves from mixed to hydrodynamic lubrication state as the sliding speed increases. The non-textured reference surface shows the lowest friction coefficient in the low contact-pressure region because the lubricant retained in the micro-dimples does not come out in the contact region. This is due to the lack of hydrodynamic lift effect as the depth of micro-dimples is greater than 10 μm.

As the contact pressure increases above 50 MPa, as shown in Figs. 11(b) and 11(c), the textured surfaces show a low friction coefficient as compared to the non-textured reference specimen. With the increase in contact pressure, the friction coefficient for the non-textured specimen remains stable and does not change with the increase in sliding speed in starved lubrication conditions. However, the friction coefficient of the textured surfaces decreases with the increase in sliding speed, attains a minimum value, and maintains this condition until the end of the test, as shown in Figs. 11(b) and 11(c). This is due to the release of lubricant by the micro-dimples in the contact region with the increase in hydrodynamic lift effect by the increase in contact pressure value.

This phenomenon of the release of lubricant is known as the "secondary lubrication effect" due to the presence of micro-dimples. However, different micro-dimple shapes have different variation in their friction coefficient values with respect to the increase in sliding speed. The micro-dimple represented by case 4 shows a stable friction coefficient variation under all contact pressure conditions and does not show any abrupt variation with the increase in sliding speed.

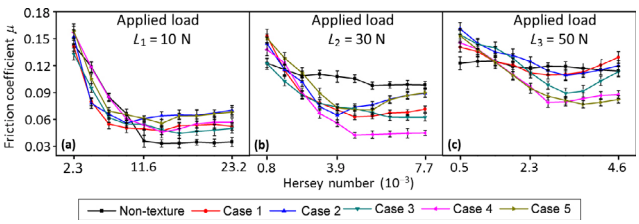

Fig. 11 Effect of micro-dimple shape on friction coefficient at constant applied load: (a) 10 N, (b) 30 N, and (c) 50 N.

4.2 Influence of surface texture density

The effects of the surface texture density on the tribological performance with different micro-dimple shapes and in different contact pressure conditions are shown in Figs. 12, 13, and 14. Stribeck curves at a contact pressure of 36 MPa are shown in Fig. 12 for all five micro-dimple geometries. It is observed that in the low contact pressure region below 50 MPa, irrespective of the surface texture density, the non-textured reference specimen shows lower friction coefficient than textured surfaces for all the micro-dimple geometries.

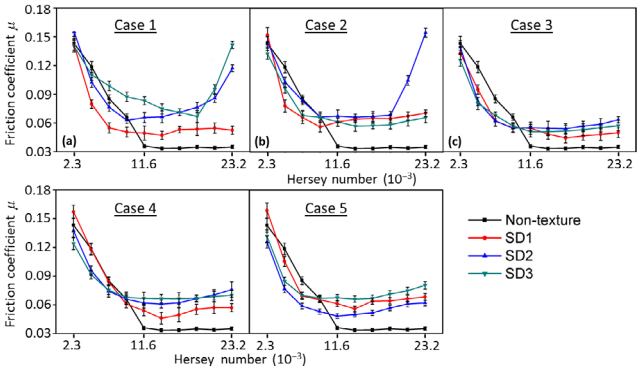

Fig. 12 Effect of surface texture density on friction coefficient at applied load of 10 N: (a) Case 1, (b) Case 2, (c) Case 3, (d) Case 4, and (e) Case 5.

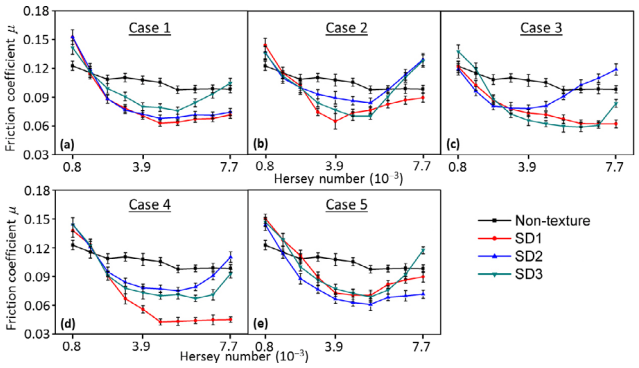

Fig. 13 Effect of surface texture density on friction coefficient at applied load of 30 N: (a) Case 1, (b) Case 2, (c) Case 3, (d) Case 4, and (e) Case 5.

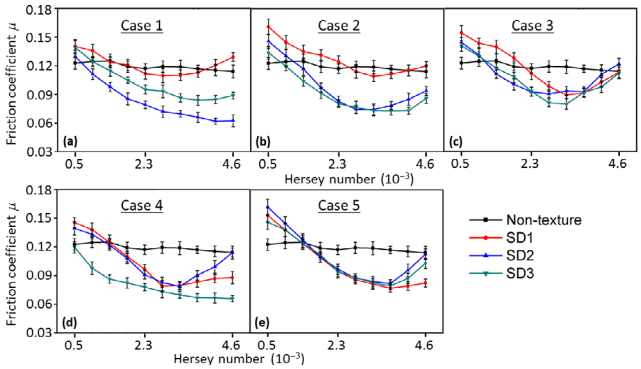

Fig. 14 Effect of surface texture density on friction coefficient at applied load of 50 N: (a) Case 1, (b) Case 2, (c) Case 3, (d) Case 4, and (e) Case 5.

With an increase in contact pressure, the textured surfaces with high texture density (SD1) show a low friction coefficient as compared to non-textured and low texture-density surface, as presented in Figs. 13 and 14. This is due to the release of retained lubricant by the micro-dimples in the contact region as the increase in contact pressure generates additional hydrodynamic lift force. In addition, the friction performance of the micro-dimple textured surfaces is improved with the increase in micro-dimple length, with optimum results being achieved for micro-dimples with the manufacturing conditions in Case 4, as shown in Fig. 13.

With a further increase in the contact pressure to 82 MPa, as shown in Fig. 14, the behavior of the textured surfaces becomes unstable. Textured surfaces at low texture density show a low friction coefficient with smaller micro-dimples, while the higher texture-density surfaces show improved friction performance with larger micro-dimple shapes. Also, a sharp increase in the friction coefficient is observed for the textured surfaces in the high sliding-speed regions. This indicates the beginning of the boundary contact region for the experimental surfaces.

4.3 Influence of dual-frequency vibration hierarchical micro-dimple

Stribeck curves obtained when using dual-frequency vibration and low-frequency vibration only to make a micro-dimple textured surface over the tested range of contact pressure are shown in Fig. 15. It is observed that with the increase in micro-dimple size, the friction performance of the hierarchical micro-dimples become better than that of low-frequency vibration only micro-dimples for low contact-pressure region. A similar trend is observed with the increase in contact pressure. In Cases 4 and 5, the hierarchical micro-dimples have a lower friction coefficient for all the contact pressure conditions than those of low-frequency-only micro-dimples.

As there are no foreign materials or bulges observed around the micro-dimple surface, this reduction in friction coefficient is attributed to the presence of hierarchical structures inside the primary surface. Due to these hierarchical structures, the cavitation pressure inside the micro-dimple is reduced, and the net hydrodynamic lift effect is increased as compared

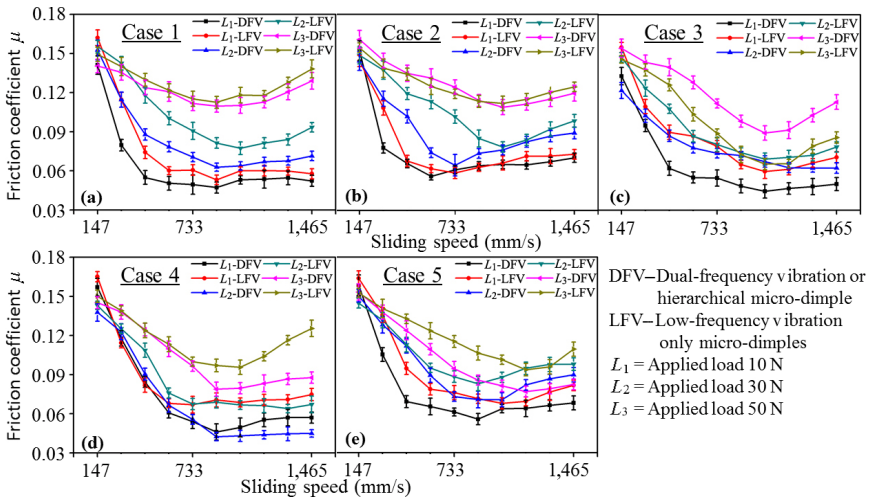

Fig. 15 Stribeck curves for dual-frequency vibration and low-frequency vibration only micro-dimples: (a) Case 1, (b) Case 2, (c) Case 3, (d) Case 4, and (e) Case 5.

to low-frequency-only micro-dimples. This increase in hydrodynamic lift improves the secondary lubrication effect by the hierarchical micro-dimples as compared to the low-frequency vibration-only micro-dimples.

4.4 Discussion

An experimental analysis was performed to examine the feasibility of hierarchical micro-dimple textured surfaces in starved lubrication conditions. Because of the complexity associated with the hierarchical micro-scale structures, the results are expected to show only the trends of the micro-dimple geometric parameters, surface texture density, and contact pressure (applied load) conditions on the friction characteristics. A dual-frequency vibration surface texturing method was used to generate micro-dimples on a cylindrical specimen with a uniform distribution. As all the micro-dimples processed at a selected manufacturing condition have uniform geometric parameters, the present manufacturing process is stable and efficient.

The friction behavior of the textured surfaces was superior to that of the non-textured reference surface when the contact pressure was above 50 MPa. As in the low contact-pressure conditions, the lubricant did not come out of the micro-dimples due to insufficient hydrodynamic lift. Since there were no bulges present around the micro-dimples, as observed from the micro-dimple profiles along the feed and cutting direction, the entrapment of the bulge particles inside the micro-dimples during the initial running-in phase of the tribology test was ruled out [25]. This also strengthened the reason for insufficient hydrodynamic lift for the lower friction coefficient of textured surfaces in a low contact-pressure region [26]. Textured surfaces with a higher surface texture density show improved friction performance as compared to low texture-density surfaces. This is due to the quantity of lubricant supplied (i.e., the secondary lubrication effect) in the contact region being greater as the actual number of micro-dimples in the contact region is higher with high texture density surfaces [27].

A comparison of the friction characteristics of hierarchical and low-frequency vibration-only micro-dimple textured surfaces was performed. It was observed that the hierarchical micro-dimples had a lower friction coefficient than the low-frequency vibration-only micro-dimples. The reason for this is the presence of hierarchical micro-nano structures in the primary surface profile of the micro-dimple. These hierarchical structures reduce the possibility of cavitation by dividing the primary surface into numerous small surfaces. These small surfaces act independently and maintain a small constant pressure well above the cavitation pressure of the liquid lubricant [28]. Thus, a net positive pressure effect is generated, which increases the net hydrodynamic lift effect. Due to the increase in hydrodynamic lift, more lubricant comes out of the micro-dimples into the contact region, and the friction coefficient is reduced.

There is a predominant presence of shape effect in the micro-dimple textured surfaces. The friction performance of the textured surfaces improves with the increase in the micro-dimple length. This trend is in line with the postulations of previous researchers [29], which states that in a case of hierarchical multi-scale texture, the bigger the size of the texture, the lower the friction coefficient is as the secondary lubrication effect is greater with bigger micro-dimples.

In summary, the present study demonstrates that the introduction of hierarchical micro-nano structures in the primary micro-dimple surface on the circumference of a cylindrical specimen is an efficient method of improving the friction performance in starved lubrication conditions. Despite the better friction characteristics of the non-textured specimen in the low contact-pressure region, the hierarchical micro-dimple textured surfaces have enhanced friction performance in the high contact-pressure regions. This is due to the increased supply of lubricant in the contact region and the lower contact ratio between the mating surfaces. This results in a lower friction coefficient for the cylinder liner material and can have benefits in applications where Al6061−T6 alloys are used as a cylinder surface.

5 Conclusions

A dual-frequency surface texturing method was used for the generation of the hierarchical micro-dimples on a cylindrical surface to examine the tribological performance. The research was mainly focused on the effects of the hierarchical micro-dimples on the

friction performance of Al6061–T6 alloy under starved lubrication conditions. Loads, sliding speeds, micro-dimple shapes, and surface-texture densities were varied to examine their influences on the tribological performance by observing the variation of Stribeck curves.

1) The friction characteristics of the hierarchical micro-dimple surface are similar to the non-textured surface when the contact pressure has low value in starved lubrication.

2) In the region of high contact-pressure (i.e., when the applied load increases during the tribological test), the hierarchical micro-dimples have lower friction coefficient than the non-textured reference specimen with the increase in the sliding speed.

3) Generation of additional hydrodynamic lift and the secondary lubrication effect due to the presence of secondary nano-structures in the hierarchical micro-dimples help in improving the tribological performance, as compared to the micro-dimples generated by low-frequency vibration only.

4) Textured surfaces with a higher surface texture density show improved tribological performance as the number of micro-dimples in the contact area is higher, due to which the secondary lubrication effect is higher.

5) A predominant presence of shape effect has been observed in the tribological performance of micro-dimple textured surfaces as the bigger micro-dimples show a lower friction coefficient as compared to the small micro-dimples.

Acknowledgements

This work is supported by the 2020 Yeungnam University research grant.

References

[1] Malshe A P, Bapat S, Rajurkar K P, Haitjema H. Bio-inspired textures for functional applications. *CIRP Ann* **67**(2): 627–650 (2018)

[2] Bixler G D, Bhushan B. Fluid drag reduction with shark-skin riblet inspired microstructured surfaces. *Adv Funct Mater* **23**(36): 4507–4528 (2013)

[3] Koch K, Bhushan B, Jung Y C, Barthlott W. Fabrication of artificial lotus leaves and significance of hierarchical structure for superhydrophobicity and low adhesion. *Soft Matter* **5**(7): 1386 (2009)

[4] Xu Y F, Zheng Q, Abuflaha R, Olson D, Furlong O, You T, Zhang Q Q, Hu X G, Tysoe W T. Influence of dimple shape on tribofilm formation and tribological properties of textured surfaces under full and starved lubrication. *Tribol Int* **136**: 267–275 (2019)

[5] Etsion I. Improving tribological performance of mechanical components by laser surface texturing. *Tribol Lett* **17**(4): 733–737 (2004)

[6] Lu P, Wood R J K. Tribological performance of surface texturing in mechanical applications—A review. *Surf Topogr: Metrol Prop* **8**(4): 043001 (2020)

[7] Grützmacher P G, Profito F J, Rosenkranz A. Multi-scale surface texturing in tribology—Current knowledge and future perspectives. *Lubricants* **7**(11): 95 (2019)

[8] Costa H L, Hutchings I M. Some innovative surface texturing techniques for tribological purposes. *Proc Inst Mech Eng Part J J Eng Tribol* **229**(4): 429–448 (2015)

[9] Kurniawan R, Ali S, Park K M, Li C P, Ko T J. Development of a three-dimensional ultrasonic elliptical vibration transducer (3D-UEVT) based on sandwiched piezoelectric actuator for micro-grooving. *Int J Precis Eng Manuf* **20**(7): 1229–1240 (2019)

[10] Kurniawan R, Kumaran S T, Ali S, Nurcahyaningsih D A, Kiswanto G, Ko T J. Experimental and analytical study of ultrasonic elliptical vibration cutting on AISI 1045 for sustainable machining of round-shaped microgroove pattern. *Int J Adv Manuf Technol* **98**(5–8): 2031–2055 (2018)

[11] Zhou X Q, Zuo C M, Liu Q, Wang R Q, Lin J Q. Development of a double-frequency elliptical vibration cutting apparatus for freeform surface diamond machining. *Int J Adv Manuf Technol* **87**(5–8): 2099–2111 (2016)

[12] Yuan Y J, Zhang D W, Jing X B, Ehmann K F. Freeform surface fabrication on hardened steel by double frequency vibration cutting. *J Mater Process Technol* **275**: 116369 (2020)

[13] Guo P, Lu Y, Ehmann K F, Cao J. Generation of hierarchical micro-structures for anisotropic wetting by elliptical vibration cutting. *CIRP Ann* **63**(1): 553–556 (2014)

[14] Kurniawan R, Ko T J, Ping L C, Kumaran S T, Kiswanto G, Guo P, Ehmann K F. Development of a two-frequency, elliptical-vibration texturing device for surface texturing. *J Mech Sci Technol* **31**(7): 3465–3473 (2017)

[15] Ali S, Kurniawan R, Ko T J. Development of 3D resonant elliptical vibration transducer for dual-frequency micro-dimple surface texturing. *Int J Precis Eng Manuf* **22**(8): 1365–1379 (2021)

[16] Kong C Y, Soar R C, Dickens P M. Characterisation of aluminium alloy 6061 for the ultrasonic consolidation process. *Mater Sci Eng A* **363**(1–2): 99–106 (2003)

[17] Kumar P K, Kumar A S. Investigation of frictional characteristics of laser textured aluminium 6061 and aluminium 7071 alloys under dry sliding conformal contact in pin on disc tribometer. *Mater Today Proc* **45**: 670–676 (2021)

[18] Tang M K, Zhang Q X, Guo Z, Yu J G, Li X W, Huang X J. A universal laser marking approach for treating aluminum alloy surfaces with enhanced anticorrosion, hardness and reduced friction. *RSC Adv* **5**(23): 18057–18066 (2015)

[19] Pavithran B, Swathanandan J, Praveen N, Kumar S R P, Kumaran D S. Study of mechanical and tribological properties of Al-6061 reinforced with silicon carbide and graphite particles. *Int J Tech Enhan Emerg Engg Res* **3**(4): 60–64 (2015)

[20] Zou Y S, Zhou K, Wu Y F, Yang H, Cang K, Song G H. Structure, mechanical and tribological properties of diamond-like carbon films on aluminum alloy by arc ion plating. *Vacuum* **86**(8): 1141–1146 (2012)

[21] John H B I. Application of average stress criterion to fracture of aluminium alloys used in aerospace applications. *Arab J Sci Eng* **39**(2): 1409–1415 (2014)

[22] Xu Y F, Zheng Q, You T, Yao L L, Hu X G. Laser-induced improvement in tribological performances of surface coatings with MoS_2 nanosheets and graphene. *Surf Coat Technol* **358**: 353–361 (2019)

[23] Luo Z H, Yu J Y, Xu Y F, Xi H, Cheng G, Yao L L, Song R H, Dearn K D. Surface characterization of steel/steel contact lubricated by PAO6 with novel black phosphorus nanocomposites. *Friction* **9**(4): 723–733 (2021)

[24] Xu Y F, Zheng Q, Geng J, Dong Y H, Tian M, Yao L L, Dearn K D. Synergistic effects of electroless piston ring coatings and nano-additives in oil on the friction and wear of a piston ring/cylinder liner pair. *Wear* **422–423**: 201–211 (2019)

[25] Lu X B, Khonsari M M. An experimental investigation of dimple effect on the stribeck curve of journal bearings. *Tribol Lett* **27**(2): 169–176 (2007)

[26] Greiner C, Schäfer M. Bio-inspired scale-like surface textures and their tribological properties. *Bioinspir Biomim* **10**(4): 044001 (2015)

[27] Mishra S P, Polycarpou A A. Tribological studies of unpolished laser surface textures under starved lubrication conditions for use in air-conditioning and refrigeration compressors. *Tribol Int* **44**(12): 1890–1901 (2011)

[28] Hamilton D B, Walowit J A, Allen C M. A theory of lubrication by microirregularities. *J Basic Eng* **88**(1): 177–185 (1966)

[29] Schneider J, Djamiykov V, Greiner C. Friction reduction through biologically inspired scale-like laser surface textures. *Beilstein J Nanotechnol* **9**: 2561–2572 (2018)

Saood ALI. He received his M.S. degree from Motilal Nehru National Institute of Technology (MNNIT) Allahabad India. He received his Ph.D. degree in mechanical engineering from Yeungnam University, Republic of Korea. He is currently a research professor at Yeungnam University, Republic of Korea. His research interests are surface texturing, tribology, hierarchical surface texture fabrication, vibration assisted machining, and ultrasonic device development for surface texturing.

Rendi KURNIAWAN. He received the S.T. degree from Universitas Indonesia, Indonesia. He received his M.S., Eng., and Ph.D. degrees in mechanical engineering from Yeungnam University, Republic of Korea. He is currently an assistant professor at Yeungnam University, Republic of Korea. His research interests include actuator studies, surface texturing, tribology, micro-dimple fabrication, elliptical vibration texturing, and vibration-assisted cutting.

Gun CHUL. He received his B.S. degree from Keimyung University, Republic of Korea. He received his M.S. degree from Yeungnam University, Republic of Korea. Now he is a Ph.D. student in mechanical engineering at Yeungnam University, Republic of Korea. His research interests are surface texturing using piezo electric actuator, tribological studies, and friction reduction.

Tae Jo KO. He received his bachelor's and M.S. degrees from Pusan National University, Republic of Korea. He received his Ph.D. degree in mechanical engineering from Pohang University of Science and Technology, Republic of Korea. Now he is a professor of mechanical engineering at Yeungnam University, Republic of Korea. His research interests include the development of machine tools, micro-cutting process, non-traditional machining, surface texturing using grinding, bio-machining, hybrid electric discharge machining (EDM) milling process, textured surface on cutting tools, and deburring process of carbon fiber reinforced polymer (CFRP) composite.